Spin-orbit effect on strong-field ionization of krypton

Robin Santra, Robert W. Dunford, and Linda Young
Argonne National Laboratory, Argonne, Illinois 60439, USA
(Received 26 July 2006; published 6 October 2006)

A recent pump-probe experiment employing tunable, linearly polarized x rays demonstrated that Kr^+ ions produced via strong-field ionization in a linearly polarized laser field are aligned, but that the degree of alignment is greatly overestimated by nonrelativistic strong-field ionization models. An effective one-electron model of strong-field ionization is presented that includes the effect of spin-orbit interaction. The method makes use of a flexible finite-element basis set and determines ionization rates in this square-integrable basis using a complex absorbing potential. It is found that even at the electric-field strength corresponding to the saturation intensity for the ionization of Kr, there is very little mixing between the $4p_{3/2}$ and $4p_{1/2}$ outer-valence orbitals. This shows that the uncoupled m_l, m_s projection quantum numbers are inappropriate to describe the Kr^+ states that are populated by strong-field ionization of krypton. For the x-ray probe step, a description is developed, within a density-matrix formalism. It is demonstrated that the inclusion of spin-orbit interaction in the ionization process provides satisfactory agreement with the experimental observation. Possibilities for time-resolved studies utilizing fs and sub-fs laser pulses are indicated.

DOI: 10.1103/PhysRevA.74.043403 PACS number(s): 32.80.Rm, 31.15.−p, 32.10.Fn

I. INTRODUCTION

Within the last four decades, an impressive body of knowledge has accumulated on the nature of the interaction of an intense laser pulse with an atom or molecule [1–18]. Traditionally, the interaction process is characterized by fragmentation products generated in the strong laser field. The electronic structure and the alignment properties of the residual ion typically remain unobserved.

A central prediction of the tunneling ionization theory by Ammosov, Delone, and Krainov [6] is a very strong dependence of the ionization rate on the orbital angular momentum projection m_l of the tunneling electron. If we consider, for instance, a noble gas atom with a ns^2np^6 valence electron configuration exposed to a laser field that is linearly polarized along the z axis, then it would be expected that an electron in the np_z orbital is ionized much faster than an electron in either np_x or np_y. This is because at sufficiently low photon energy and sufficiently high laser intensity, so that the Keldysh or adiabaticity parameter [19] is of order 1 or a little less, ionization takes place via tunneling through the potential barrier arising from the superposition of the atomic potential and the quasistatic potential associated with the laser electric field. The np_z electron has the highest probability of being found in the direction of minimum tunneling barrier width. It therefore tunnels fastest.

Ion alignment in tunnel ionization was addressed in connection with the question as to the efficiency of ionization of atoms at relativistic laser intensities [20,21]. It was argued that any depletion of the $m_l=0$ sublevel would impede the production of higher charge states during the laser pulse, unless there is a mechanism that repopulates the $m_l=0$ sublevel on a time scale that is short in comparison to the laser period. The experimental result of Gubbini *et al.* [21] is consistent with extremely fast m_l dealignment. This conclusion is based on a comparison between the experimentally observed charge states and the charge states calculated with the ADK formula [6]. Thus, using this methodology, in combination with ultraintense laser pulses, no indication of residual ion alignment was found.

A recent pump-probe experiment at the Advanced Photon Source (APS) at Argonne National Laboratory provided direct evidence for ion alignment in tunnel ionization [22]. At the same time, it was shown in this experiment that the degree of alignment is not consistent with the nonrelativistic tunneling picture.

A linearly polarized 800-nm laser pulse with an energy of 2.0 mJ, a pulse duration of 40 fs, and a focal width of 100 μm (FWHM) served as the pump. The laser-produced ions were probed using a linearly polarized hard x-ray pulse (duration about 100 ps) from the APS. The x-rays were focused within the laser volume to a width of 10 μm (FWHM). The x-ray microprobe technique described in Ref. [22] allowed for a time-resolved, tomographic analysis of the ions produced by the laser. The noble gas species investigated was krypton. At the laser intensity employed, mostly Kr^+ was produced. The Kr^+ ions were probed via x-ray absorption at a photon energy of 14.313 keV. At this energy, an electron in the K shell can be resonantly excited into the laser-produced hole in the $4p$ shell. The resulting hole in the K shell relaxes on a subfemtosecond time scale through the emission of a characteristic $K\alpha$ x ray, which was detected in order to monitor the absorption of the probe x rays. The alignment of the $4p$ hole was observed by measuring the resonant x-ray absorption of Kr^+ as a function of the angle between the x-ray and laser polarizations. The ratio between the absorption probability in the parallel and perpendicular polarization configurations was found to be about 2:1. This ratio is much smaller than what might be expected on the basis of the ADK model.

The purpose of this paper is to provide a theoretical framework for the pump-probe experiment carried out at the APS and to point out interesting implications for future studies using ultrashort (a few femtoseconds or shorter) pump and probe pulses. An important insight gained from our analysis is that, in the heavier noble gas atoms, atomic spin-orbit coupling has a substantial impact on the ionization dy-

namics in a strong laser field (even at nonrelativistic intensities). This may have implications for our understanding of such technologically relevant phenomena as high-order harmonic generation, where theories currently neglect relativistic atomic effects [16,23,24].

In Sec. II, we elaborate on the specific approach we have chosen to treat the problem of strong-field ionization taking into account spin-orbit coupling. The main message of Sec. II is that the nonrelativistic m_l, m_s quantum numbers are inadequate to describe the ionization of Kr in a strong laser field. The interaction with the laser electric field does not render the spin-orbit coupling negligible. A density-matrix formulation is employed in Sec. III to explore the polarization dependence of resonant x-ray absorption by the laser-produced ions. It is demonstrated that the Kr^+ state population determined in Sec. II allows us to understand the alignment properties observed in the APS experiment [22]. Section IV concludes. Atomic units are used throughout, unless otherwise noted.

II. STRONG-FIELD IONIZATION OF KRYPTON

As mentioned in the Introduction, according to the nonrelativistic tunnel ionization picture underlying the ADK model [6], a linearly polarized laser field preferentially ionizes the $4p$, $m_l=0$ subshell of Kr. (The polarization axis is taken as the quantization axis.) Tunnel ionization of the $4p$, $m_l=\pm 1$ subshells is suppressed. Taïeb, Véniard, and Maquet calculate that 95% of Kr^+ ions generated in a strong optical field are in the $m_l=0$ substate [20]. This would suggest that if the laser intensity is just high enough to saturate the ionization of neutral krypton, then a strongly aligned sample of Kr^+ ions would be produced. More precisely, the ratio between the resonant x-ray absorption probability in the parallel and perpendicular polarization configurations (see the Introduction) would be expected to be $95/2.5=38$. (If, say, p_x lies along the laser/x-ray propagation direction, then only p_y can be probed in the perpendicular polarization configuration. That is the reason why 95 must be compared with 2.5, not 5.)

Two objections may be raised to this expectation. First, at 800 nm, it takes only 10 photons to ionize either the $4p_{3/2}$ shell (binding energy $I_{3/2}=14.0$ eV) or the $4p_{1/2}$ shell ($I_{1/2}=14.7$ eV) of Kr. Indeed, it has been argued [25,26] that strong-field ionization of krypton at a laser wavelength of 617 nm is best described in terms of multiphoton ionization, i.e., the tunneling picture is not entirely appropriate. In order to test whether the multiphoton ionization mechanism would imply substantially reduced ion alignment, we performed nonrelativistic multiphoton ionization calculations using the Floquet-type technique described in Ref. [27]. We found that the ratio of 10-photon ionization cross sections $\sigma^{(10)}(m_l=0)/\sigma^{(10)}(m_l=\pm 1)$ is 10:1 at 800 nm. Hence, no matter whether the tunneling or the multiphoton picture of strong-field ionization of Kr is adopted, nonrelativistic models predict a much more pronounced Kr^+ x-ray absorption anisotropy than observed experimentally [22].

Relativistic corrections to the electron dynamics driven by the laser field (see, for instance, Ref. [28]) are not important at intensities of the order of 10^{14} W/cm^2 (i.e., peak electric field strengths of the order of 0.1 a.u.). The intraatomic dynamics may, however, be affected by relativistic effects. This brings us to the second objection that can be raised against the expectation of strong Kr^+ alignment: The spin-orbit splitting between the $4p_{3/2}$ and $4p_{1/2}$ states of Kr^+ is relatively large (0.7 eV), so that the m_l quantum numbers may not be sufficiently well conserved during strong-field ionization. To investigate this possibility, we have developed an effective one-particle description of tunnel ionization with the inclusion of spin-orbit interaction.

The basis of this model is the Hamiltonian

$$H = -\frac{1}{2}\nabla^2 + V_{\mathrm{HS}}(r) + \frac{1}{2}\alpha^2\frac{1}{r}\frac{dV_{\mathrm{HS}}}{dr}\boldsymbol{l}\cdot\boldsymbol{s} - z\mathcal{E} - i\eta W(r). \quad (1)$$

The effective one-electron potential V_{HS} is calculated using the Hartree-Fock-Slater [29,30] code written by Herman and Skillman [31]. (Applications of the Herman-Skillman potential to atomic photoionization are discussed, for example, in Refs. [27,32–34].) V_{HS} describes the interaction of an electron with the nucleus and with the mean-field generated by the other electrons. In addition to the Hartree-Fock-Slater approach itself, a key approximation made here is that the external electric field $\mathcal{E}$ is too weak to substantially modify the intraatomic potential represented by V_{HS}. At field strengths of 0.1 a.u. or less, this approximation should be reasonable. (We calculate that the average electric field seen by a $4p$ electron in the Kr Herman-Skillman potential is about 37 a.u.) Note that $\mathcal{E}$ in Eq. (1) represents a *static* field along the z axis. The strategy in the following is to use Eq. (1) to calculate, as a function of $\mathcal{E}$, the tunnel ionization rates $\gamma(\mathcal{E})$ of the $4p$-type orbitals of Kr. Intensity-dependent ionization rates are then obtained by averaging $\gamma(\mathcal{E})$ over a laser period. The operator in Eq. (1) depending on the scalar product of the orbital angular momentum $\boldsymbol{l}$ and the spin $\boldsymbol{s}$ of the active electron describes the spin-orbit interaction (α is the fine-structure constant). The last operator in Eq. (1) $-i\eta W$ is a complex absorbing potential (CAP) [35–50]. The real, nonnegative parameter η is the CAP strength. The local one-electron potential $W(r)$ is chosen here as

$$W(r) = \begin{cases} 0, & 0 \leqslant r < c, \\ (r-c)^2, & r \geqslant c, \end{cases} \quad (2)$$

where $c=4$ a.u. in this paper. This choice places the absorbing potential right outside the ionic core. The CAP absorbs the tunnel-ionized electron and renders the associated wave function square integrable. The CAP approach is closely related to the technique of (exterior) complex scaling [51–57]. In the one-electron problem, it does not really matter whether the CAP or the complex-scaling approach is selected. For molecular many-electron problems, however, using a CAP has proved advantageous. See, for example, Refs. [46,47,58–60].

Let

$$H_0 = -\frac{1}{2}\nabla^2 + V_{\mathrm{HS}}(r). \quad (3)$$

Using a radial finite-element basis [61–67] consisting of 3001 finite-element basis functions, we calculate for orbital

angular momentum quantum numbers $l=0,\ldots,11$ the 75 energetically lowest radial eigenfunctions of H_0 that vanish at both ends of the radial grid. The quadratically spaced grid extends from $r=0$ to $r=60$ a.u. (All numerical parameters here and in the following are chosen such as to ensure converged tunnel ionization rates.) Because of the boundary conditions adopted, the spectrum of H_0 is discrete and we may write the eigenstates of H_0 as $|n,l,m_l,m_s\rangle$ and the associated eigenvalues as $E_{n,l}$. (Note that V_{HS} is spherically symmetric.) By allowing the spin-orbit coupling operator in Eq. (1) to act only within the $2(2l+1)$-dimensional n,l subspace (first-order degenerate perturbation theory), a diagonal representation of the field- and CAP-free Hamiltonian is obtained:

$$\left[-\frac{1}{2}\nabla^2 + V_{\mathrm{HS}}(r) + \frac{1}{2}\alpha^2\frac{1}{r}\frac{dV_{\mathrm{HS}}}{dr}\boldsymbol{l}\cdot\boldsymbol{s}\right]|n,l,j,m\rangle = E_{n,l,j}|n,l,j,m\rangle, \tag{4}$$

where

$$|n,l,j,m\rangle = \sum_{m_l,m_s} C(lsj;m_l m_s m)|n,l,m_l,m_s\rangle \tag{5}$$

and

$$E_{n,l,j} = E_{n,l} + \frac{\Delta E^{(\mathrm{SO})}_{n,l}}{2l+1}\begin{cases} l, & j=l+1/2, \\ -l-1, & j=l-1/2. \end{cases} \tag{6}$$

$C(lsj;m_l m_s m)$ is a Clebsch-Gordan coefficient [68], and $\Delta E^{(\mathrm{SO})}_{n,l}$ stands for the fine-structure splitting of the n,l subshell. In order to make sure that within our model the $4p_{3/2}$ and $4p_{1/2}$ binding energies agree with the experimental values, we set $\Delta E^{(\mathrm{SO})}_{4p}=0.666$ eV and choose the exchange parameter [30,31] underlying the Herman-Skillman calculation as 1.1035. In this way, $E_{4p}=-14.222$ eV, which equals the energy of the spin-orbit-unperturbed $4p$ level that is derived from Eq. (6). Since the singular nature of the spin-orbit interaction tends to amplify inaccuracies of the Herman-Skillman wave functions near $r=0$, we calculate $\Delta E^{(\mathrm{SO})}_{n,l}$ for higher lying levels using a hydrogenic formula [69]

$$\Delta E^{(\mathrm{SO})}_{n,l} = \frac{\mathrm{const}}{n^3 l(l+1)}. \tag{7}$$

The constant in this model is 85.248 eV, to reproduce the experimental $4p$ fine-structure splitting.

A matrix representation of the full Hamiltonian H [Eq. (1)] is constructed now with respect to the state vectors $|n,l,j,m\rangle$. The matrix elements of the dipole operator z are determined using standard angular momentum algebra [70]

$$\begin{aligned}\langle n,l,j,m|z|n',l',j',m'\rangle &= \delta_{m,m'}(-1)^{j+l+s}\sqrt{(2j+1)(2l+1)} \\ &\times C(j1j';m0m)\begin{Bmatrix} j & j' & 1 \\ l' & l & s \end{Bmatrix} \\ &\times C(l1l';000)\int_0^\infty u_{n,l}(r) r u_{n',l'}(r)dr.\end{aligned} \tag{8}$$

Here, $u_{n,l}(r)$ is a radial eigenfunction of H_0 $[u_{n,l}(0)=0]$. The quantity in curly braces is a $6-j$ symbol [70]. An immediate consequence of Eq. (8) is that the external electric field does not give rise to direct coupling matrix elements among the $|4p_j,m\rangle$ states. On the other hand, because of the presence of this external electric field, the only conserved quantum number is the total angular momentum projection m. The matrix of the spherically symmetric CAP is diagonal with respect to three of the four quantum numbers n,l,j,m:

$$\langle n,l,j,m|W|n',l',j',m'\rangle = \delta_{l,l'}\delta_{j,j'}\delta_{m,m'} \times \int_0^\infty u_{n,l}(r)W(r)u_{n',l}(r)dr. \tag{9}$$

The complex Siegert energy E [71–76] of each resonance state of interest is calculated by diagonalizing the matrix of H (exploiting the conservation of m) and optimizing [39] the parameter η characterizing the strength of the CAP. The imaginary part of the Siegert energy is a direct measure of the ionization rate $\gamma=-2\,\mathrm{Im}(E)$. For numerical efficiency, the CAP-free Hamiltonian matrix—a real symmetric matrix—is diagonalized first. A subset of 300 eigenvectors is selected (based on their overlap with the field-unperturbed $4p$ eigenstates), and the optimization of η is performed by diagonalizing the complete complex symmetric Hamiltonian in the selected subspace [47].

TABLE I. Stark shifts $\Delta E^{(\mathrm{Stark})}$ and tunnel ionization rates γ of the $4p$ orbitals of krypton, at an electric field strength of $\mathcal{E}=0.10$ a.u. Each metastable state can be labeled in terms of the projection quantum number m. (Data were calculated for positive m. Replacing m with $-m$ yields identical results.) Also shown are the squared overlaps $|c(j=1/2)|^2$ and $|c(j=3/2)|^2$ of the field-perturbed resonance states with the field-free $4p$ eigenstates.

m	$\Delta E^{(\mathrm{Stark})}$ (a.u.)	γ (a.u.)	$\lvert c(j=1/2)\rvert^2$	$\lvert c(j=3/2)\rvert^2$
+1/2	-1.25×10^{-2}	4.89×10^{-3}	0.976	0.016
+1/2	-1.41×10^{-2}	1.18×10^{-2}	0.022	0.957
+3/2	-1.42×10^{-2}	1.41×10^{-3}	0	0.970

The results of such a calculation, at $\mathcal{E}=0.10$ a.u., are listed in Table I. If this electric field strength is interpreted as the amplitude of a linearly polarized laser field, the corresponding intensity is 3.5×10^{14} W/cm^2. Note that this is already a little higher than the saturation intensity for the ionization of krypton at 800 nm [77]. In spite of this relatively high electric field strength (which a neutral Kr atom is unlikely to actually experience), Table I illustrates that the field-free quantum number j can still be used to label the field-perturbed resonance states rather accurately. There is very little mixing between $|4p_{1/2},m=\pm1/2\rangle$ and $|4p_{3/2},m=\pm1/2\rangle$. In other words, the spin-orbit interaction is, effectively, not weak in comparison to the interaction with the external electric field. A reason for this is that the external electric field does not directly couple the $4p$ states to each other, as pointed out above in connection with Eq. (8). The Stark shifts of the $|4p_j,m\rangle$ states are all of similar magnitude and smaller than the fine-structure splitting. Not only is j a virtually conserved quantum number, the fine-structure splitting remains almost unaffected by the external electric

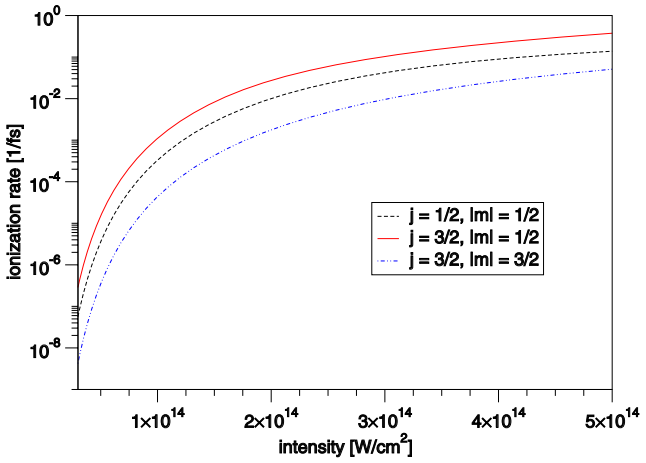

FIG. 1. (Color online) Cycle-averaged ionization rates of the $4p$ orbitals of krypton as a function of laser intensity, calculated for linearly polarized light.

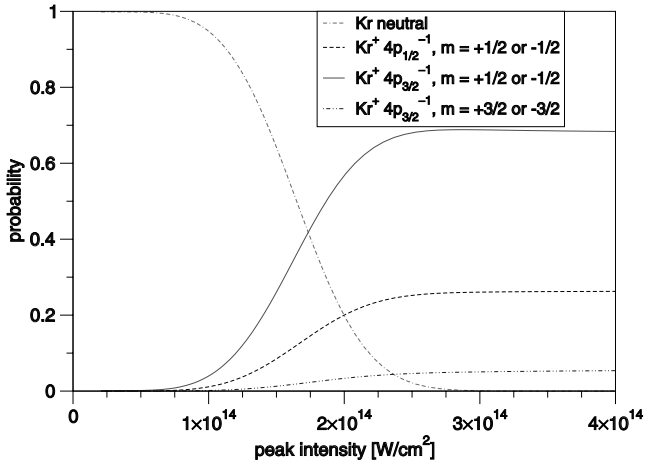

FIG. 2. Probability, as a function of peak intensity, of finding either neutral Kr or the $4p$-type states of Kr^+ after exposure of neutral krypton to a laser pulse of Gaussian temporal shape (FWHM 40 fs). $4p_j^{-1}$ in the figure legend means that a hole is present in the $4p_j$ orbital.

field—the fine-structure splitting decreases by only 7%—and is resolvable within the ionization widths $\gamma_{j,m}$ of the field-perturbed states $|4p_j,m\rangle$. We observe that $\gamma_{3/2,\pm 1/2}$ is greater than $\gamma_{3/2,\pm 3/2}$ by more than a factor of 8 and greater than $\gamma_{1/2,\pm 1/2}$ by 2.4. This can be rationalized on the basis of the nonrelativistic tunneling picture: Tunneling is much faster for $|4p,m_l=0,m_s\rangle$ than for $|4p,m_l=\pm 1,m_s\rangle$. $|4p_{3/2},m=\pm 3/2\rangle$ has no overlap with $|4p,m_l=0,m_s\rangle$, while the squared overlap with $|4p,m_l=0,m_s\rangle$ is two times greater for $|4p_{3/2},m=m_s\rangle$ than for $|4p_{1/2},m=m_s\rangle$.

The total atomic ionization rate is obtained as the sum over all $\gamma_{j,m}$ weighted by the number of electrons in the respective j,m subshell. Combining the data in Table I, the ionization rate of Kr, at $\mathcal{E}=0.10$ a.u., is 0.036 a.u., which corresponds to a tunneling lifetime of 0.67 fs. Relevant in the case of a laser field is the rate averaged over a laser period (in fact, a suitably chosen quarter period is sufficient):

$$\bar{\gamma}_{j,m} = \frac{2}{\pi}\int_0^{\pi/2} \gamma_{j,m}(\mathcal{E}_0 \cos\varphi)d\varphi. \tag{10}$$

The relation between the field amplitude $\mathcal{E}_0$ and the intensity I in the case of a linearly polarized laser field is $\mathcal{E}_0=\sqrt{8\pi\alpha I}$, where the intensity is measured in units of $E_H/(t_0 a_0^2)=6.436\,41\times 10^{15}$ W/cm^2 (E_H is the Hartree energy; t_0 is the atomic unit of time; a_0 is the Bohr radius). In Fig. 1, the cycle-averaged rates $\bar{\gamma}_{j,m}$ are plotted as a function of intensity.

We are now in a position to calculate the state distribution of Kr^+ ions generated by a laser pulse. Since the x-ray microprobe technique [22] allows one to selectively measure the ions produced in the immediate vicinity of the laser focus, we do not perform any spatial averaging in the following. If the laser pulse envelope changes slowly on the time scale of the laser period, which was to a good approximation the case in the experiment described in Ref. [22], then we can use the cycle-averaged tunneling rates and insert them into rate equations

$$\dot{\rho}_0(t) = -\sum_{j,m} \bar{\gamma}_{j,m}(t)\rho_0(t), \tag{11}$$

$$\dot{\rho}_{j,|m|}(t) = \{\bar{\gamma}_{j,m}(t) + \bar{\gamma}_{j,-m}(t)\}\rho_0(t). \tag{12}$$

Here, ρ_0 is the probability of finding a neutral krypton atom ($\rho_0=1$ before the pulse), and $\rho_{j,|m|}$ is the probability of finding Kr^+ with a hole in either the $4p_j,m$ or the $4p_j,-m$ orbital ($\rho_{j,|m|}=0$ before the pulse). Depopulation of Kr^+ due to Kr^{2+} production is not considered here. We solve the rate equations assuming a Gaussian intensity envelope with a full width at half maximum of 40 fs. The resulting Kr^+ state distribution is shown in Fig. 2 as a function of the peak intensity of the laser pulse. First, in agreement with experiment [77], the ionization of Kr saturates between 1×10^{14} W/cm^2 and 2×10^{14} W/cm^2. Second, at saturation the Kr^+ state populations are $\rho_{3/2,1/2}=69\%$, $\rho_{1/2,1/2}=26\%$, and $\rho_{3/2,3/2}=5\%$. In the following section, we will show that this state distribution allows us to understand the polarization dependence of the Kr^+ x-ray absorption observed in the APS experiment [22].

III. DENSITY-MATRIX DESCRIPTION OF X-RAY PROBE OF VALENCE HOLE

The rate equation approach employed in the previous section predicts a Kr^+ density matrix that is diagonal in the $|j,m\rangle \equiv |4p_j,m\rangle$ basis. Possible coherences are neglected. This makes sense for the conditions that were present in the APS experiment, where the pump and probe pulses were long in comparison to the valence spin-orbit period $T^{(SO)}$, which is 6.2 fs in krypton. [$T^{(SO)}$ is defined in terms of the valence fine-structure splitting: $T^{(SO)}=2\pi/\Delta E^{(SO)}$.] However, if the pump pulse is sufficiently short, then, even if the photoelectron is observed, there is no way one can decide whether the electron comes from the $4p_{3/2}$ or the $4p_{1/2}$ orbital. In other words, an ultrashort pulse of a few fs or less generates an ion that is in a coherent superposition of the

$|j,m\rangle$ states. A correspondingly short probe pulse could be used to follow the resulting spin-orbit wave-packet dynamics in a time-resolved fashion.

In the following, we consider initial density matrices (right after ionization has taken place) that are diagonal with respect to the conserved quantum number m:

$$\rho(t=0)=\sum_m \sum_{j',j''} |j',m\rangle \rho^{(m)}_{j',j''} \langle j'',m|. \tag{13}$$

This form includes initial density matrices that are diagonal in the $|j,m\rangle$ basis and those that are diagonal in the $|m_l,m_s\rangle \equiv |4p,m_l,m_s\rangle$ basis. We require that

$$\rho^{(m)}_{j',j''} = \rho^{(-m)}_{j',j''} \tag{14}$$

and

$$\mathrm{Tr}[\rho(t=0)] = \sum_{j,m} \rho^{(m)}_{j,j} = 1. \tag{15}$$

Equation (14) indicates that strong-field ionization is not sensitive to the sign of the projection quantum number, and Eq. (15) ensures normalization of the initial density matrix. Utilizing the Schrödinger-picture time-evolution operator $U(t)$, the density matrix at $t>0$ is given by

$$\rho(t) = \sum_m \sum_{j',j''} \rho^{(m)}_{j',j''} U(t)|j',m\rangle\langle j'',m|U^\dagger(t). \tag{16}$$

Employing hard x rays at a photon energy of 14.313 keV, one can probe the Kr^+ $4p$ hole by resonant x-ray absorption by a K-shell electron. The resulting core hole decays very rapidly via x-ray emission within 240 as. The decay width of the core hole is referred to in the following as Γ. In order to describe the probe process, we determine the probability $P(t)$ of absorbing an x-ray photon

$$P(t) = 1 - \sum_{j,m} \langle j,m|\rho(t)|j,m\rangle. \tag{17}$$

To this end, we define

$$\Xi^{(m)}_{j'',j'}(t) = \delta_{j'',j'} - \sum_{j,\tilde{m}} \langle j'',m|U^\dagger(t)|j,\tilde{m}\rangle\langle j,\tilde{m}|U(t)|j',m\rangle, \tag{18}$$

so that

$$P(t) = \sum_m \sum_{j',j''} \rho^{(m)}_{j',j''} \Xi^{(m)}_{j'',j'}(t). \tag{19}$$

$\Xi^{(m)}_{j'',j'}(t)$ is most efficiently evaluated in the interaction picture using time-dependent perturbation theory, treating the atomic Hamiltonian H_0 (including spin-orbit interaction) as the unperturbed part and the interaction with the probe x rays as the perturbation. The perturbation is described semiclassically employing a time-dependent interaction $V(t)$. Thus, to second order in perturbation theory,

$$\Xi^{(m)}_{j'',j'}(t) = \langle j'',m|O(t)+O^\dagger(t)|j',m\rangle, \tag{20}$$

where

$$O(t) = \int_0^t dt' e^{iH_0t'} V(t') e^{-iH_0t'} \int_0^{t'} dt'' e^{iH_0t''} V(t'') e^{-iH_0t''}. \tag{21}$$

We now calculate an explicit expression for $\Xi^{(m)}_{j'',j'}(t)$ using the electric dipole approximation (nondipole effects in Kr $1s$ photoionization are not very strong [78]) and assuming the following time-dependent interaction:

$$V(t) = -(\boldsymbol{d}\cdot\boldsymbol{\varepsilon}_p)\mathcal{E}_p \cos(\omega_p t) \begin{cases} 1, & 0 \leqslant t_1 \leqslant t < t_2, \\ 0, & \text{otherwise}. \end{cases} \tag{22}$$

Here, $\boldsymbol{d}$ is the electric dipole operator, $\boldsymbol{\varepsilon}_p$ is the polarization vector of the linearly polarized probe x rays, $\mathcal{E}_p$ is the electric field amplitude of the x rays, and ω_p is the x-ray photon energy. The x-ray pulse starts at $t=t_1$ and ends at $t=t_2$. We assume that the decay of the core hole is faster than the duration of the probe pulse $[\Gamma(t_2-t_1)\gg 1]$. We further assume that ω_p is tuned to the $1s$-$4p$ resonance and exploit that, within the decay width of the core hole, the $4p_{1/2}$ and $4p_{3/2}$ states of Kr^+ are energetically indistinguishable. Hence, after the probe pulse $(t>t_2)$,

$$\Xi^{(m)}_{j'',j'}(t) = \frac{\mathcal{E}_p^2}{\Gamma} T^{(m)}_{j'',j'} f_{j'',j'}(t_1,t_2), \tag{23}$$

where

$$T^{(m)}_{j'',j'} = \sum_{m_K} \langle j'',m|\boldsymbol{d}\cdot\boldsymbol{\varepsilon}_p|K,m_K\rangle\langle K,m_K|\boldsymbol{d}\cdot\boldsymbol{\varepsilon}_p|j',m\rangle. \tag{24}$$

In this expression, $|K,m_K\rangle$ stands for the resonantly core-excited state with projection quantum number m_K. The angular momentum quantum number j_K ($j_K=1/2$ for a hole in the K shell) is not explicitly written.

The delay t_1 and the duration $\tau=t_2-t_1$ of the probe pulse enter in Eq. (23) through $f_{j'',j'}(t_1,t_2)$. We do not give the most general expression for $f_{j'',j'}(t_1,t_2)$, but consider two specific scenarios. In the first scenario, t_1 and t_2 vary from shot to shot by amounts comparable to or larger than $T^{(\mathrm{SO})}$, so that after averaging over the corresponding phases

$$f^{[1]}_{j'',j'} = \delta_{j'',j'}\langle\tau\rangle. \tag{25}$$

$\langle\tau\rangle$ is the average pulse duration. This is the case for experiments using currently available synchrotron radiation sources. In the second scenario, the probe pulse is short in comparison to the spin-orbit period. The delay t_1 is controlled from shot to shot to within a fraction of $T^{(\mathrm{SO})}$. Analogous conditions must be satisfied by the pump pulse. In this case, using $E_j \equiv E_{4p,j}$,

$$f^{[2]}_{j'',j'} = \exp\{\mathrm{i}(E_{j''}-E_{j'})t_1\}\tau. \tag{26}$$

We note that the matrix elements $T^{(m)}_{j'',j'}$, and thus the x-ray absorption probability P, depend on the spatial orientation of the x-ray polarization vector $\boldsymbol{\varepsilon}_p$. Let ϑ_p denote the angle between the quantization axis (i.e., the laser polarization axis) and the x-ray polarization vector. Then, applying standard angular momentum algebra [70] and making explicit

use of the one-particle quantum numbers of the hole in the initial and final states, the following $\boldsymbol{T}^{(m)}$ matrices are found from Eq. (24):

$$\boldsymbol{T}^{(+3/2)} = \varkappa \begin{pmatrix} 0 & 0 \\ 0 & \frac{1}{2}\sin^2\vartheta_p \end{pmatrix}, \tag{27}$$

$$\boldsymbol{T}^{(+1/2)} = \varkappa \begin{pmatrix} \frac{1}{3} & \sqrt{2}\left(\frac{1}{2}\sin^2\vartheta_p - \frac{1}{3}\right) \\ \sqrt{2}\left(\frac{1}{2}\sin^2\vartheta_p - \frac{1}{3}\right) & \frac{2}{3} - \frac{1}{2}\sin^2\vartheta_p \end{pmatrix}, \tag{28}$$

and

$$T^{(m)}_{j'',j'} = (-1)^{j''-j'} T^{(-m)}_{j'',j'}. \tag{29}$$

In Eqs. (27) and (28), the first column and row refers to $j=1/2$, the second to $j=3/2$. The parameter

$$\varkappa = \frac{1}{3}|\langle s\|d\|p\rangle|^2 \tag{30}$$

is defined in terms of the reduced dipole matrix element $\langle s\|d\|p\rangle$ between the core (s) and valence (p) orbitals. $\langle s\|d\|p\rangle$ refers to purely spatial one-electron wave functions.

Collecting the results obtained in Eqs. (19), (23), and (25)–(29), we find the x-ray absorption probabilities for the two scenarios considered above [see Eqs. (25) and (26)]. Thus, in the case of scenario 1 (poor temporal control of the pump and probe pulses on the time scale of the spin-orbit period), the x-ray absorption probability is

$$P^{[1]} = \frac{\mathcal{E}_p^2}{\Gamma}\varkappa\langle\tau\rangle\left\{\frac{1}{3}\rho_{1/2,1/2} + \left(\frac{2}{3} - \frac{1}{2}\sin^2\vartheta_p\right)\rho_{3/2,1/2} + \frac{1}{2}\sin^2\vartheta_p\rho_{3/2,3/2}\right\}, \tag{31}$$

where, in correspondence to Eq. (12),

$$\rho_{j,|m|} = \rho^{(m)}_{j,j} + \rho^{(-m)}_{j,j}. \tag{32}$$

$P^{[1]}$ is a periodic function of ϑ_p with a period of 180°. Therefore, in order to characterize the polarization-dependent x-ray absorption in terms of a quantity that is independent of parameters such as $\varkappa$ and $\langle\tau\rangle$, we form the ratio of $P^{[1]}$ at $\vartheta_p=0°$ and $\vartheta_p=90°$:

$$R^{[1]} = \frac{P^{[1]}(\vartheta_p = 0°)}{P^{[1]}(\vartheta_p = 90°)} = \frac{2\rho_{1/2,1/2} + 4\rho_{3/2,1/2}}{2\rho_{1/2,1/2} + \rho_{3/2,1/2} + 3\rho_{3/2,3/2}}. \tag{33}$$

We draw two important conclusions from this equation. First, if the populations $\rho_{j,|m|}$ are allowed to vary arbitrarily (subject to the conditions that $\rho_{j,|m|}\geqslant 0$ and $\rho_{1/2,1/2}+\rho_{3/2,1/2}+\rho_{3/2,3/2}=1$), the observable ratio $R^{[1]}$ in the first scenario can assume any value between 0 ($\rho_{3/2,3/2}=1$) and 4 ($\rho_{3/2,1/2}=1$). Greater values, however, are not possible. This is in stark contrast to what would be expected if it were possible to neglect spin-orbit coupling. Second, using the populations $\rho_{3/2,1/2}=69\%$, $\rho_{1/2,1/2}=26\%$, and $\rho_{3/2,3/2}=5\%$ calculated in Sec. II, $R^{[1]}=2.4$. This is still a little higher than the experimentally observed ratio of 2.0 at a peak intensity of 4×10^{14} W/cm^2 [22], but in view of the simplicity of the model developed in this paper, the level of agreement is good. This signals that the inclusion of spin-orbit interaction in the tunneling picture is crucial. Two factors not included in our description may be particularly important in explaining the small remaining discrepancy: One is that the relative population of $|1/2,\pm1/2\rangle$ may be somewhat too small. This may be the case because, as mentioned in Sec. II, it requires the same number of photons (at 800 nm) to ionize either $4p_{3/2}$ or $4p_{1/2}$, whereas the tunneling model suppresses the ionization of the more strongly bound $4p_{1/2}$ orbital. The second factor is that at the relatively high peak intensity of 4×10^{14} W/cm^2, some 10% of the Kr^+ ions are ionized and give rise to Kr^{2+}. The presence of Kr^{2+} may lead to further reduction of $R^{[1]}$.

For the second scenario, where the pump-pulse duration and the shot-to-shot fluctuations of probe-pulse delay and duration (fixed t_1 and τ) are small in comparison to $T^{(SO)}$, the exact form of the initial density matrix $\rho(t=0)$ depends on details of the pump pulse. All that can be said at this point is that for a sufficiently short pump pulse, the density matrix is initially not diagonal in the $|j,m\rangle$ basis. One interesting possibility, which might be realized experimentally, is an initial density matrix that is diagonal in the uncoupled $|m_l,m_s\rangle$ basis. In this case, exploiting that strong-field ionization probes the sign of neither m_l nor m_s, only one independent parameter characterizes $\rho(t=0)$, which we may choose as the probability W_0 of generating Kr^+ with $m_l=0$ ($m_s=\pm1/2$). Using the inverse of Eq. (5), the density-matrix coefficients $\rho^{(m)}_{j',j''}$, which are needed for evaluating Eq. (19), can be expressed in terms of W_0. Thus, the x-ray absorption probability as a function of the time delay t_1 is

$$P^{[2]} = \frac{\mathcal{E}_p^2}{\Gamma}\varkappa\tau\left\{\left[W_0\left(\frac{1}{3} - \frac{1}{2}\sin^2\vartheta_p\right) + \frac{1}{6}\sin^2\vartheta_p\right] \times[1 + 2\cos(\Delta E^{(SO)}t_1)] + \frac{2}{9}[1 - \cos(\Delta E^{(SO)}t_1)]\right\}. \tag{34}$$

Hence, the ratio of $P^{[2]}(\vartheta_p=0°)$ and $P^{[2]}(\vartheta_p=90°)$ is

$$R^{[2]} = \frac{6W_0[1 + 2\cos(\Delta E^{(SO)}t_1)] + 4[1 - \cos(\Delta E^{(SO)}t_1)]}{3(1 - W_0)[1 + 2\cos(\Delta E^{(SO)}t_1)] + 4[1 - \cos(\Delta E^{(SO)}t_1)]}. \tag{35}$$

$R^{[2]}$ is a periodic function of t_1 with period $T^{(SO)}$. $R^{[2]}$ vs t_1 is plotted in Fig. 3 for the case $W_0=95\%$ (see Sec. II). The figure illustrates how the time-resolved determination of $R^{[2]}$ would provide a direct measure of the spin-orbit dynamics of the laser-generated hole in the krypton valence shell.

IV. CONCLUSIONS

Pump-probe techniques are established tools in ultrafast science, but they represent a rather novel approach in the

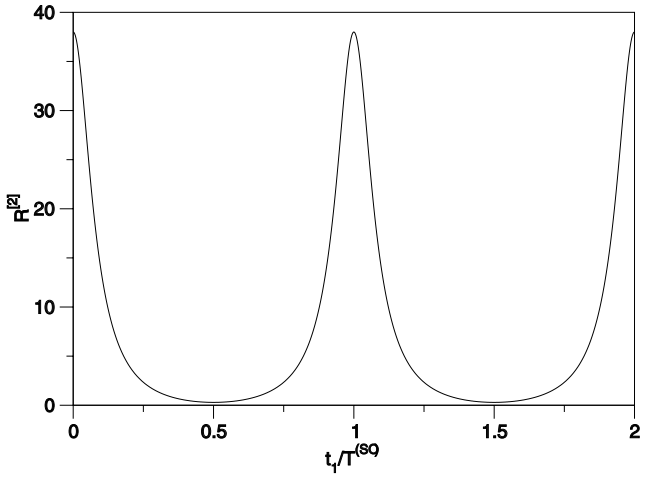

FIG. 3. $R^{[2]}$ [Eq. (35)] as a function of the probe delay t_1 in units of the spin-orbit period $T^{(SO)}$. In the experiment suggested by the figure, the resonant x-ray absorption by a tunnel-ionized noble gas atom (Ne, Ar, Kr, Xe) would be measured for two different angles ϑ_p between the (pump) laser and (probe) x-ray polarizations. $R^{[2]}$ is the ratio of the absorption probabilities at $\vartheta_p=0°$ and $\vartheta_p=90°$.

x-ray physics of atoms and molecules, primarily due to the current lack of ultrafast, high-flux x-ray sources. Future x-ray free-electron lasers, such as the Linac Coherent Light Source (LCLS) currently under construction at the Stanford Linear Accelerator Center, are expected to open a new door to ultrafast science. One of the motivations underlying the x-ray microprobe technology [22] is the development of the techniques required for measurements at LCLS. But even with relatively long x-ray pulses, x-ray-based pump-probe experiments reveal new scientific insights.

A recent experiment at the Advanced Photon Source [22] has, for the first time, provided information on the alignment properties of krypton ions generated via strong-field ionization. The degree of alignment was found to be far lower than expected on the basis of nonrelativistic tunneling or multiphoton models. We have shown in this paper that the spin-orbit effect has a large impact on the Kr^+ alignment and can explain the experimental observation. It is particularly important to emphasize that at the electric-field strength at which Kr ionizes, there is hardly any mixing of the $4p_{3/2}$ and $4p_{1/2}$ orbitals. The Kr^+ density matrix is essentially diagonal in the $|4p_j,m\rangle$ basis. This means that, in general, strong-field ionization of Kr does not produce a coherent superposition of the $|4p_j,m\rangle$ states.

Creating such a spin-orbit wave packet requires a laser pulse that is shorter than the spin-orbit period. The creation of such a wave packet- and the time-resolved measurement of its dynamics—represents an intriguing challenge for future studies. The formal analysis presented in this paper is not restricted to krypton. It applies, in principle, to all noble gas atoms (except helium), even though the degree of $p_{3/2}$, $p_{1/2}$ mixing in the laser electric field is likely to be greater in the lighter noble gases than in krypton. In order to explore the spin-orbit-induced wave-packet dynamics of the valence hole in a time-resolved fashion, there are practical considerations that may render other noble gas species more suitable than krypton. In Table II, the spin-orbit period, the photon energy for the resonant transition of an electron from the K shell into the outer-valence hole (np), and the photon energy for the resonant transition of an electron from the inner-valence shell (ns) into the outer-valence hole are shown for Ne, Ar, Kr, and Xe. The entries in the table are based on data taken from Refs. [79–84].

TABLE II. The table shows the spin-orbit period $T^{(SO)}$ for an outer-valence hole in the noble gas atoms Ne, Ar, Kr, and Xe. The spin-orbit period is inversely proportional to the splitting between the $p_{3/2}$ and $p_{1/2}$ fine-structure components of the outer-valence hole. Also shown is the energy $E_{K\text{-ov}}$ that is required to resonantly excite a K-shell electron into the outer-valence hole. $E_{\text{iv-ov}}$ is the energy difference between inner- and outer-valence shells. $E_{\text{iv-ov}}$ is the average of the respective transition energies for the $p_{3/2}$ and $p_{1/2}$ outer-valence components.

	$T^{(SO)}$ (fs)	$E_{K\text{-ov}}$ (keV)	$E_{\text{iv-ov}}$ (eV)
Ne	42.7	0.85	26.9
Ar	23.3	3.19	13.4
Kr	6.2	14.3	13.2
Xe	3.2	34.5	10.7

We note that the requirements in terms of pump and probe pulse durations are least stringent in the case of Ne. An intense 800-nm, few-fs laser pulse would work well to launch a spin-orbit wave packet in Ne^+. For the heavier noble gases, in particular Kr and Xe, the pump pulse would have to be not only intense, but less than a femtosecond long. If the $1s$-$2p$ transition is selected to probe the dynamics of the neon $2p$ hole, then an 849-eV, few-fs pulse would have to be available. The resonant transition could be monitored by observing the Auger decay of the core hole. Such an experiment will become feasible in a few years when the first x-ray free-electron laser, the Linac Coherent Light Source, comes online at Stanford. (The initial pulse duration is expected to be of the order of a few hundred femtoseconds, but the eventual production of few-fs pulses is expected [85].) An alternative approach is to use the $2s$-$2p$ transition at a photon energy of 26.9 eV. This lies in the vacuum ultraviolet, so that one might consider employing high-order harmonic generation in order to supply a 26.9-eV, few-fs probe pulse. Then it might be most efficient to detect the resonant $2s$-$2p$ excitation by measuring the vuv fluorescence from the $2s$ hole. Experiments along these lines would allow one to explore the emergence of coherence in the ion density matrix as the laser pulse duration is shortened. They might serve as a fundamental testing ground for our ability to coherently control the dynamics of atomic electrons using ultrashort laser pulses.

ACKNOWLEDGMENTS

We thank Stephen H. Southworth, Louis F. DiMauro, and Ariel Gordon for discussions. This work was supported by the Office of Basic Energy Sciences, Office of Science, U.S. Department of Energy, under Contract No. W-31-109-ENG-38.

[1] L. V. Keldysh, Zh. Eksp. Teor. Fiz. **47**, 1945 (1964) [Sov. Phys. JETP **20**, 1307 (1965)].
[2] F. H. M. Faisal, J. Phys. B **6**, L89 (1973).
[3] L. A. Lompre, G. Mainfray, C. Manus, S. Repoux, and J. Thebault, Phys. Rev. Lett. **36**, 949 (1976).
[4] H. R. Reiss, Phys. Rev. A **22**, 1786 (1980).
[5] P. Lambropoulos, Phys. Rev. Lett. **55**, 2141 (1985).
[6] M. V. Ammosov, N. B. Delone, and V. P. Krainov, Zh. Eksp. Teor. Fiz. **91**, 2008 (1986) [Sov. Phys. JETP **64**, 1191 (1986)].
[7] F. Yergeau, S. L. Chin, and P. Lavigne, J. Phys. B **20**, 723 (1987).
[8] R. R. Freeman, P. H. Bucksbaum, H. Milchberg, S. Darack, D. Schumacher, and M. E. Geusic, Phys. Rev. Lett. **59**, 1092 (1987).
[9] S. Augst, D. Strickland, D. D. Meyerhofer, S. L. Chin, and J. H. Eberly, Phys. Rev. Lett. **63**, 2212 (1989).
[10] P. B. Corkum, N. H. Burnett, and F. Brunel, Phys. Rev. Lett. **62**, 1259 (1989).
[11] A. Huillier, K. J. Schafer, and K. C. Kulander, Phys. Rev. Lett. **66**, 2200 (1991).
[12] U. Mohideen, M. H. Sher, H. W. K. Tom, G. D. Aumiller, O. R. Wood II, R. R. Freeman, J. Boker, and P. H. Bucksbaum, Phys. Rev. Lett. **71**, 509 (1993).
[13] P. B. Corkum, Phys. Rev. Lett. **71**, 1994 (1993).
[14] B. Walker, B. Sheehy, L. F. DiMauro, P. Agostini, K. J. Schafer, and K. C. Kulander, Phys. Rev. Lett. **73**, 1227 (1994).
[15] T. E. Glover, J. K. Crane, M. D. Perry, R. W. Lee, and R. W. Falcone, Phys. Rev. Lett. **75**, 445 (1995).
[16] T. Brabec and F. Krausz, Rev. Mod. Phys. **72**, 545 (2000).
[17] M. Drescher, M. Hentschel, R. Kienberger, M. Ulberacker, V. Yakovlev, A. Scrinzi, T. Westerwalbesloh, U. Kleineberg, U. Heinzmann, and F. Krausz, Nature (London) **419**, 803 (2002).
[18] J. Itatani, J. Levesque, D. Zeidler, H. Niikura, H. Pépin, J. C. Kieffer, P. B. Corkum, and D. M. Villeneuve, Nature (London) **432**, 867 (2004).
[19] N. B. Delone and V. P. Krainov, *Multiphoton Processes in Atoms* (Springer, Berlin, 2000).
[20] R. Taïeb, V. Véniard, and A. Maquet, Phys. Rev. Lett. **87**, 053002 (2001).
[21] E. Gubbini, U. Eichmann, M. Kalashnikov, and W. Sandner, Phys. Rev. Lett. **94**, 053602 (2005).
[22] L. Young, D. A. Arms, E. M. Dufresne, R. W. Dunford, D. L. Ederer, C. Höhr, E. P. Kanter, B. Krässig, E. C. Landahl, E. R. Peterson, J. Rudati, R. Santra, and S. H. Southworth, Phys. Rev. Lett. **97**, 083601 (2006).
[23] M. Lewenstein, Ph. Balcou, M. Yu. Ivanov, A. L'Huillier, and P. B. Corkum, Phys. Rev. A **49**, 2117 (1994).
[24] A. Gordon and F. X. Kärtner, Phys. Rev. Lett. **95**, 223901 (2005).
[25] E. Mevel, P. Breger, R. Trainham, G. Petite, P. Agostini, J. P. Chambaret, A. Migus, and A. Antonetti, J. Phys. B **25**, L401 (1992).
[26] E. Mevel, P. Breger, R. Trainham, G. Petite, P. Agostini, A. Migus, J. P. Chambaret, and A. Antonetti, Phys. Rev. Lett. **70**, 406 (1993).
[27] R. Santra and C. H. Greene, Phys. Rev. A **70**, 053401 (2004).
[28] M. W. Walser, D. J. Urbach, K. Z. Hatsagortsyan, S. X. Hu, and C. H. Keitel, Phys. Rev. A **65**, 043410 (2002).
[29] J. C. Slater, Phys. Rev. **81**, 385 (1951).
[30] J. C. Slater and K. H. Johnson, Phys. Rev. B **5**, 844 (1972).
[31] F. Herman and S. Skillman, *Atomic Structure Calculations* (Prentice-Hall, Englewood Cliffs, N.J., 1963).
[32] J. W. Cooper, Phys. Rev. **128**, 681 (1962).
[33] S. T. Manson and J. W. Cooper, Phys. Rev. **165**, 126 (1968).
[34] J. J. Yeh and I. Lindau, At. Data Nucl. Data Tables **32**, 1 (1985).
[35] A. Goldberg and B. W. Shore, J. Phys. B **11**, 3339 (1978).
[36] G. Jolicard and E. J. Austin, Chem. Phys. Lett. **121**, 106 (1985).
[37] G. Jolicard and E. J. Austin, Chem. Phys. **103**, 295 (1986).
[38] D. Neuhauser and M. Baer, J. Chem. Phys. **90**, 4351 (1989).
[39] U. V. Riss and H.-D. Meyer, J. Phys. B **26**, 4503 (1993).
[40] U. V. Riss and H.-D. Meyer, J. Phys. B **28**, 1475 (1995).
[41] N. Moiseyev, J. Phys. B **31**, 1431 (1998).
[42] U. V. Riss and H.-D. Meyer, J. Phys. B **31**, 2279 (1998).
[43] J. P. Palao, J. G. Muga, and R. Sala, Phys. Rev. Lett. **80**, 5469 (1998).
[44] J. P. Palao and J. G. Muga, J. Phys. Chem. A **102**, 9464 (1998).
[45] H. O. Karlsson, J. Chem. Phys. **109**, 9366 (1998).
[46] R. Santra, L. S. Cederbaum, and H.-D. Meyer, Chem. Phys. Lett. **303**, 413 (1999).
[47] R. Santra and L. S. Cederbaum, J. Chem. Phys. **115**, 6853 (2001).
[48] R. Santra and L. S. Cederbaum, Phys. Rep. **368**, 1 (2002).
[49] R. Santra and L. S. Cederbaum, J. Chem. Phys. **117**, 5511 (2002).
[50] J. G. Muga, J. P. Palao, B. Navarro, and I. L. Egusquiza, Phys. Rep. **395**, 357 (2004).
[51] J. Aguilar and J. M. Combes, Commun. Math. Phys. **22**, 269 (1971).
[52] E. Balslev and J. M. Combes, Commun. Math. Phys. **22**, 280 (1971).
[53] T. N. Rescigno, C. W. McCurdy, and A. E. Orel, Phys. Rev. A **17**, 1931 (1978).
[54] W. P. Reinhardt, Annu. Rev. Phys. Chem. **33**, 223 (1982).
[55] C. W. McCurdy, T. N. Rescigno, E. R. Davidson, and J. G. Lauderdale, J. Chem. Phys. **73**, 3268 (1980).
[56] N. Moiseyev, Phys. Rep. **302**, 212 (1998).
[57] T. N. Rescigno, M. Baertschy, W. A. Isaacs, and C. W. McCurdy, Science **286**, 2474 (1999).
[58] R. Santra, J. Zobeley, and L. S. Cederbaum, Chem. Phys. Lett. **324**, 416 (2000).
[59] R. Santra, J. Zobeley, L. S. Cederbaum, and N. Moiseyev, Phys. Rev. Lett. **85**, 4490 (2000).
[60] S. Feuerbacher, T. Sommerfeld, R. Santra, and L. S. Cederbaum, J. Chem. Phys. **118**, 6188 (2003).
[61] K. J. Bathe, *Finite Element Procedures in Engineering Analysis* (Prentice Hall, Englewood Cliffs, NJ, 1976).
[62] K. J. Bathe and E. Wilson, *Numerical Methods in Finite Element Analysis* (Prentice Hall, Englewood Cliffs, NJ, 1976).
[63] M. Braun, W. Schweizer, and H. Herold, Phys. Rev. A **48**, 1916 (1993).
[64] J. Ackermann and J. Shertzer, Phys. Rev. A **54**, 365 (1996).
[65] T. N. Rescigno, M. Baertschy, D. Byrum, and C. W. McCurdy, Phys. Rev. A **55**, 4253 (1997).
[66] K. W. Meyer, C. H. Greene, and B. D. Esry, Phys. Rev. Lett. **78**, 4902 (1997).
[67] R. Santra, K. V. Christ, and C. H. Greene, Phys. Rev. A **69**, 042510 (2004).

[68] M. E. Rose, *Elementary Theory of Angular Momentum* (Dover, New York, 1995).
[69] P. Strange, *Relativistic Quantum Mechanics* (Cambridge University Press, Cambridge, 1998).
[70] A. R. Edmonds, *Angular Momentum in Quantum Mechanics* (Princeton University Press, Princeton, New Jersey, 1996).
[71] A. J. F. Siegert, Phys. Rev. **56**, 750 (1939).
[72] R. G. Newton, *Scattering Theory of Waves and Particles* (Dover, Mineola, NY, 2002).
[73] R. M. More and E. Gerjuoy, Phys. Rev. A **7**, 1288 (1973).
[74] O. I. Tolstikhin, V. N. Ostrovsky, and H. Nakamura, Phys. Rev. Lett. **79**, 2026 (1997).
[75] O. I. Tolstikhin, V. N. Ostrovsky, and H. Nakamura, Phys. Rev. A **58**, 2077 (1998).
[76] R. Santra, J. M. Shainline, and C. H. Greene, Phys. Rev. A **71**, 032703 (2005).
[77] H. Maeda, M. Dammasch, U. Eichmann, W. Sandner, A. Becker, and F. H. M. Faisal, Phys. Rev. A **62**, 035402 (2000).
[78] B. Krässig, J.-C. Bilheux, R. W. Dunford, D. S. Gemmell, S. Hasegawa, E. P. Kanter, S. H. Southworth, L. Young, L. A. LaJohn, and R. H. Pratt, Phys. Rev. A **67**, 022707 (2003).
[79] Richard D. Deslattes, Ernest G. Kessler, Jr., P. Indelicato, L. de Billy, E. Lindroth, and J. Anton, Rev. Mod. Phys. **75**, 35 (2003).
[80] W. Persson, Phys. Scr. **3**, 133 (1971).
[81] C. Yamada, H. Kanamori, and E. Hiroita, J. Chem. Phys. **83**, 552 (1985).
[82] L. Minnhagen, J. Opt. Soc. Am. **61**, 1257 (1971).
[83] J. Sugar and A. Musgrove, J. Phys. Chem. Ref. Data **20**, 861 (1991).
[84] J. E. Hansen and W. Persson, Phys. Scr. **36**, 602 (1987).
[85] P. Emma, K. Bane, M. Cornacchia, Z. Huang, H. Schlarb, G. Stupakov, and D. Walz, Phys. Rev. Lett. **92**, 074801 (2004).